Supplementary Information

# Three-dimensional numerical simulation and experimental investigation of boundary-driven streaming in surface acoustic wave microfluidics

Chuyi Chen,[a] Steven Peiran Zhang,[a] Zhangming Mao,[b] Nitesh Nama,[b] Yuyang Gu,[a] Po-Hsun Huang,[a] Yun Jing,[c] Xiasheng Guo,*[d] Francesco Costanzo,*[b] and Tony Jun Huang*[a]


[a.] Department of Mechanical Engineering and Material Science, Duke University, NC 27707, USA. Email: tony.huang@duke.edu

[b.] Department of Engineering Science and Mechanics, The Pennsylvania State University, University Park, PA 16802, USA. Email: costanzo@engr.psu.edu

[c.] Department of Mechanical and Aerospace Engineering, North Carolina State University, Raleigh, NC 27695-7910, USA.

[d.] Key Laboratory of Modern Acoustics (MOE), Department of Physics, Collaborative Innovation Center of Advanced Microstructure, Nanjing University, Nanjing 210093, China. Email: guoxs@nju.edu.cn

## Part 1. 2D Validation of the "Slip Velocity Method"

To validate that the slip velocity method yields consistent solutions, a simple 2D problem (Fig. S1) is solved by both the traditional approach and slip velocity method. The corresponding two results are compared by calculating the convergence function.
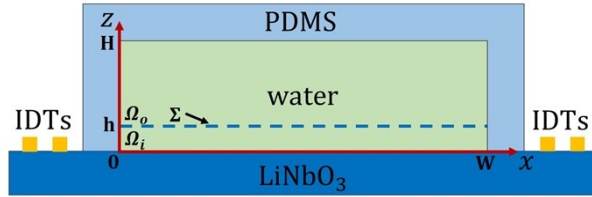


**Fig. S1** Cross-section of the channel in the classic standing surface acoustic wave (SAW) device. A PDMS channel filled with water is bonded between a pair of interdigital transducers (IDTs) fabricated on a LiNbO$_3$ substrate. The green domain indicates the computational domain, a rectangular water domain of width W and height H. The blue dashed line indicates the position of top of the Stokes boundary layer ($\Sigma$) with a thickness of h. $\Omega_i$ and $\Omega_o$ are the inner streaming domain and outer streaming domain, respectively.

**Table 1** Parameters used in the simulation[1,2] (at 298K).

| | | |
|---|---|---|
| Density of water | $\rho_0$ | 997 kg/m³ |
| Speed of sound in water | $c_0$ | 1495 m/s |
| Dynamic viscosity of water | $\mu$ | $8.9 \times 10\bar{\text{Pa}}^4$ s |
| Kinematic viscosity of water | $\nu$ | 8.93    m²/s 10 |
| Speed of sound in LiNbO$_3$ | $c_s$ | 3900 m/s |
| Density of PDMS | $\rho_P$ | 970 kg/m³ |
| Speed of sound in PDMS | $c_P$ | 1080 m/s |
| Driving frequency | $f$ | 13 MHz |
| Wavelength of SAW | $\lambda$ | 300 μm |
| Displacement amplitude | $A_m$ | 0.748 nm |
| Amplitude ratio between the longitudinal and transverse vibrations of Rayleigh SAW | $\chi$ | 0.7428 |
| Displacement decay coefficient | $\alpha$ | 176 m⁻¹ |

### 1. 2D Model System

The acoustic streaming in a cross-section of the channel in a classic standing surface acoustic wave (SAW) device (Fig. S2(a)) is chosen to be studied by the two approaches here. In the device, a pair of interdigital transducers (IDTs) is fabricated on the LiNbO$_3$ substrate. The channel is made of PDMS and bonded to the substrate between the IDTs. In this study, we focus our investigation on the acoustic streaming patterns in water. Thus, the computational domain is chosen to be the rectangular water domain (the green domain in Fig. 2(a)). The driving frequency is set to be 13 MHz which corresponds to SAWs with a wavelength of λ=300 μm. The channel width (W) and height (H) are set to be 300 μm and 100 μm, respectively, in order to study the physics within just one wavelength. The governing equations for this 2D problem are Eqs. (3)-(14) stated in Section 2.2. The parameters used in this case are listed in Table S1.

### 2. Numerical Models

The numerical solution of the above-stated problem is solved via the finite element software package COMSOL Multiphysics 5.2a.

**A. Traditional Approach.** In the traditional approach, there are two steps to solve the acoustic streaming patterns in a fluid field.[1,2] In the first step, the first-order equations (Eqs. (11) and (12)) are solved to determine the first-order acoustic field in the whole fluid domain ($\Omega_i \cup \Omega_o$). Based on the first-order solution of $p_1$ and $v_1$, the mass source term and force source terms on the right side of Eqs. (13) and (14) can be determined. This solution shows the effect of the first-order acoustic field on the second-order acoustic streaming pattern. In the second step, the second-order acoustic streaming problem is solved

in the whole fluid domain ($\Omega_i \cup \Omega_o$) based on the first-order solution from the last step. This model follows the procedure in the work of Guo et al.[2] Details of the model are stated below. In the first step, a "Thermoviscous Acoustics" physics package is used to solve Eqs. (11) and (12) which govern the first-order acoustic field in $\Omega_i \cup \Omega_o$ in Fig. S1. The vibration velocity of the piezoelectric substrate is modeled by the classic analytical expression of the 2D standing Rayleigh SAW pattern[1,2]:

$$v_x = \chi A_m \omega \{ e^{i(\omega t - kx) - \alpha x} + e^{i[\omega t - k(W - x)] - \alpha(W - x)} \} \qquad (S1)$$

$$v_z = -i A_m \omega \{ e^{i(\omega t - kx) - \alpha x} - e^{i[\omega t - k(W - x)] - \alpha(W - x)} \} \qquad (S2)$$

where $\chi$ is the amplitude ratio between the longitudinal and transverse vibrations of Rayleigh SAW, $A_m$ is the amplitude of the transverse vibration displacement, and $\alpha$ is the decay coefficient of the vibration displacement along the propagating direction with a frequency of 13 MHz. The velocity expression (Eqs. (S1) and (S2)) is superimposed as the boundary condition at the substrate-water interface. A "normal impedance" boundary condition is applied to the water-PDMS interfaces. A "Frequency Domain" solver is used to solve this boundary value problem at the driving frequency 13 MHz. In the second step, a "Laminar Flow" physics package is applied to solve the second-order equations (Eqs. (13) and (14)) based on the first-order solution from the last step in $\Omega_i \cup \Omega_o$ as shown in Fig. S1. The mass source term (

$$m_s = -\nabla \cdot \langle \rho_1 v_1 \rangle$$

) and force source terms (

$$F_s = \rho_0 \left\langle \frac{\partial v_1}{\partial t} \right\rangle + \rho_0 \langle (v_1 \cdot \nabla) v_1 \rangle$$

) are superimposed in the whole domain by adding "weak contribution" and "volume force" conditions. A "No Slip Wall" boundary condition is applied to all the boundaries. At last, a "Stationary" solver is used to solve the physics of the second-order problem.

**B. Slip Velocity Method.** As shown in Fig. S1, the SAW-induced acoustic streaming in the microfluidic channel is categorized as boundary-driven streaming. Thus, the outer streaming in $\Omega_o$ can be considered as driven by the "slip velocity," which is the inner streaming distribution on the top boundary of $\Omega_i$. By applying the "slip velocity method," the solution procedure of the outer streaming pattern can be simplified to the following steps. In Step 1, the acoustic field governed by Eqs. (11) and (12) is solved in the inner streaming domain ($\Omega_i$). Then in Step 2, the inner acoustic streaming pattern is solved based on Eqs. (13) and (14) and the solution from Step 1 in $\Omega_i$. The inner acoustic streaming velocity distributed on the boundary between $\Omega_i$ and $\Omega_o$ is obtained as the slip velocity ($v_{slip}$). In Step 3, the slip velocity is applied as the boundary condition at the bottom of the bulk fluid domain ($\Omega_o$) to solve the original continuity equation and the Navier-Stokes equation (Eqs. (3) and (4)) in this domain. The velocity solution from this step in $\Omega_o$ is the outer acoustic streaming pattern. Following the steps of the "slip velocity method", the COMSOL model is set up as below. In Step 1, "Thermoviscous Acoustics" physics is applied to the Stokes boundary layer ($\Omega_i$ in Fig. S1) to solve the acoustic field governed by Eqs. (11) and (12). The velocity at the bottom (substrate-water interface) is prescribed to the expression in Eqs. (S1) and (S2) representing the vibration mode of Rayleigh SAW. The PDMS impedance is set in the "normal impedance" condition on both the left and right PDMS-water interfaces. The boundary condition on the top boundary of the Stokes boundary layer ($\Sigma$ in Fig. S1) is approximately set to be the water impedance. This physics is solved by a "Frequency Domain" solver at 13 MHz. In Step 2, a "Laminar Flow" physics is applied only to inner streaming domain ($\Omega_i$) to calculate the inner acoustic streaming pattern governed by Eqs. (13) and (14). The bottom, left, and right boundaries are set to a "no slip wall" condition. The boundary condition on top of the inner streaming domain ($\Sigma$) is set to an "outlet" with pressure equal to

zero. A "Stationary" solver is applied to find the solution of the inner acoustic streaming. In Step 3, another "Laminar Flow" physics is used to solve the normal continuity and Navier-Stokes equations (Eqs. (3) and (4)) in the bulk fluid domain upon the ($\Omega_o$). The solution of inner streaming velocity on $\Sigma$ from Step 2 is captured and applied as the slip velocity of the "slip wall" condition on the bottom of $\Omega_o$. Other boundaries of domain $\Omega_o$ are set to be a "no slip wall" condition. In the end, another "Stationary" solver provides the physics in the bulk fluid domain $\Omega_o$ and yields the outer acoustic streaming patterns.

Both models used mapped rectangular meshes. The elements' height in the Stokes boundary layer of height $h$ was set to $\delta_v/10$. Other elements in the bulk fluid are designated 0.2 µm in height. This fine mesh meets the requirement of the mesh convergence study as demonstrated by Nama et al.[1] The mesh
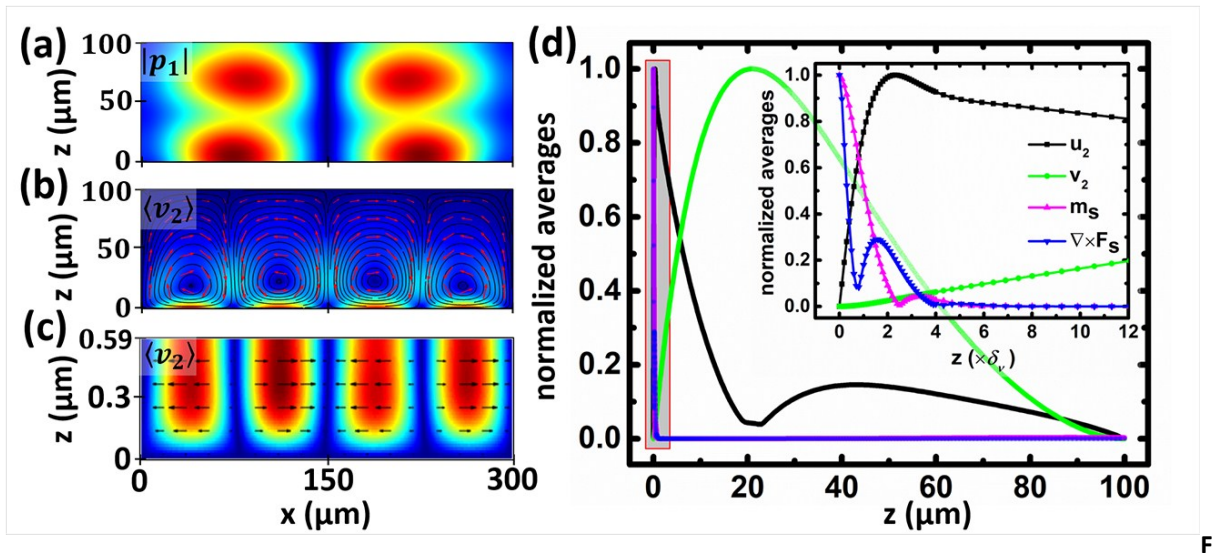


**F**

**ig. S2** Color plots of solutions from the traditional approach. (a) The absolute value of first-order pressure $p_1$ in the whole fluid domain ($\Omega_i \cup \Omega_o$). The magnitude of the value is indicated by colors ranging from zero (blue) to 0.28 MPa (red). In a channel of one wavelength in width, two pressure anti-nodes are created by the standing SAW in the horizonal direction. (b) The time-averaged second-order velocity $\langle v_2 \rangle$ in the entire fluid domain ($\Omega_i \cup \Omega_o$) with red color showing the maximum value of $4.32 \times 10^{-4}$ m/s and blue color showing the minimum value of zero. The streamlines and arrows indicate the streaming patterns and directions. Four vortices exist in the channel within one wavelength width. The streaming flows upward at the pressure nodes and flows downward at the pressure anti-nodes. The streaming velocity close to the bottom wall is much larger than elsewhere. (c) Zoomed-in, time-averaged second-order velocity $\langle v_2 \rangle$ in a layer with a thickness of $4\delta_v$ (equal to 0.588 µm when driven by a 13 MHz acoustic wave in the water) close to the bottom wall plotted in the same color range of figure (b). Indicated by the arrow, $u_2$, the horizontal component of $\langle v_2 \rangle$, with a gradient in the vertical direction, dominates the streaming patterns in this layer. The streaming velocity increases from the bottom and reaches the maximum at the top of this layer. (d) Variation of the normalized value of the line averages $g(z)$ of the absolute value of $u_2$ (x component of the time-averaged second-order velocity), $v_2$ (z component of the time-averaged second-order velocity), $m_s$ (mass source term) and $\nabla \times F_s$ (curl of the force term) with respect to the vertical position z. The $g(z)$ of $u_2$, $v_2$, $m_s$ and $\nabla \times F_s$ is normalized to their maximum of $2.715 \times 10^{-4}$ m/s at z =2.23$\delta_v$=0.338 µm, $8.681 \times 10^{-5}$ m/s at z=21.179 µm, $1.066 \times 10^{14}$ N/m⁴ at z=0 and 56.245 Pa·s/m² at z=0,

guarantees the accuracy of the solution and minimizes other errors in the verification of the slip velocity. The results are stated and discussed below.

## 3. Results and Discussion

**A. Traditional Results and Physics in the Stokes Boundary Layer.** The solution of absolute first-order pressure $p_1$ and averaged second-order velocity $\langle v_2 \rangle$ (acoustic streaming velocity) are plotted in Fig. S2(a)-(c). As shown in Fig. S2(a), two pressure antinodes generated by the standing leaky SAW distribute in the channel of one wavelength in width. Fig. S2(b) shows that the streaming velocity is relatively fast close to the bottom and decreases as the height increases. Observing the streaming near the bottom, the $\langle v_2 \rangle$ in a layer close to bottom wall with a thickness of $4^{\delta_v}$ (0.588 µm in this case) is zoomed in at Fig. S2(c). In this layer, the streaming flows almost horizontally from pressure antinodes toward nodes without vortex tendency. The streaming velocity is zero at the substrate-liquid interface due to the non-slip boundary condition, and it increases gradually away from this interface. To evaluate the variation tendency of variables in the vertical direction, the line averages of the variables are calculated. We define the line average function $\bar{g}(z)$ for a variable $g(x,z)$ to be the integration of the absolute value of $g(x,z)$ on a horizontal line at depth z in the channel divided by the channel width $W$:

$$\bar{g}(z) = \frac{\int |g(x,z)|dx}{W}. \qquad (S3)$$

The normalized line average functions for the horizontal ($u_2$) and vertical ($v_2$) components of the streaming velocity are plotted with black and green lines in Fig. S2(d), respectively. The horizontal streaming velocity increases from zero at z=0 to its maximum at around z=2.23$^{\delta_v}$ (0.338 µm), then it keeps decreasing up to the position of the vortices' centers. At the vortices' centers, it increases again and then decreases when it gets close to the top boundary. The vertical streaming velocity increases from zero at the bottom to the maximum at z=21.179 µm, which is the vertical position of the vortices' centers, and decreases to zero again at the top of the domain.

In the slip velocity method, determining the optimal thickness of the inner streaming domain ($\Omega_i$), h, is the most-essential procedure for the accuracy of the solution for two reasons. Firstly, for a computational domain in a channel with a thickness of H, the thickness of the outer streaming domain (H-h) depends on the inner streaming domain thickness (h). Secondly and most remarkably, the "slip velocity" which is captured at the interface ($\Sigma$) between the inner streaming domain ($\Omega_i$) and the outer streaming domain ($\Omega_o$) will determine the outer streaming pattern. Although the inner streaming domain corresponds to the Stokes boundary layer where the viscous attenuation effect mainly penetrates, the thickness of the Stokes boundary layer is defined as several times $\delta_v$[3,4] instead of an exact number. As shown in Fig. S2(d), the amplitude of the x component of streaming velocity $u_2$ varies sharply in the area near the oscillatory bottom wall. Thus, slightly shifting the position of $\Sigma$ will significantly change the "slip velocity" as well as the resultant outer streaming pattern. It is improper to determine either the position of $\Sigma$ as the vertical maximum of the horizontal line average of $u_2$ or as the horizontal line maximum of $u_2$, since the value of $u_2$ has the fluctuant horizontal distribution. As such, we explore the distribution of the actuations of the acoustic streaming—the mass source term ($m_s$) and the curl of the force source term ($\nabla \times F_s$). As shown by the pink line in Fig. 3(d), the line average of the absolute mass source term decreases dramatically from its maximum at z=0. In the area upon z=5$^{\delta_v}$, the

amplitude of $m_s$ is much smaller compared with the one in the area below z=$5\delta_v$. This indicates that the effect of the mass source terms is mainly confined in the area below z=$5\delta_v$. Similarly, we also find that the curl of the force source term ($\nabla \times F_s$), which is the main factor of the vortex-shape streaming, also acts mainly in this area (Fig. 3(d)). Since the mass source term and force source terms represent the effect of the first-order acoustic field on the second-order acoustic streaming, we find that this effect mainly penetrates a fluid layer close to the oscillatory bottom wall (~$5\delta_v$) and induces both the inner streaming and corresponding outer streaming. As a result, the optimal thickness of the inner streaming layer for the "slip velocity method" could be around $5\delta_v$. To verify this hypothesis, we apply the "slip velocity method" to solve the outer streaming velocities with different thicknesses of the inner streaming domain ($\Omega_i$), and we evaluate their similarities with the corresponding streaming velocity solved by the traditional approach.

**B. Convergence Analysis.** To evaluate the similarity between two solutions, a relative convergence function comparing the difference between a solution $g(x,z)$ solved by the slip velocity method and a reference solution $g_{ref}(x,z)$ solved by the traditional approach in the computational domain is defined as

$$C(g) = \sqrt{\frac{\int (g - g_{ref})^2 dV}{\int g_{ref}{}^2 dV}}, \qquad (S4)$$

where $V$ is the computational domain. A smaller convergence function value signifies a better approximation to the solution from the traditional approach. The convergence function is calculated for the following physics: the x component ($u_2$) and z component ($v_2$) of the inner streaming velocity in domain $\Omega_i$, the x component ($u_{slip}$) and z component ($v_{slip}$) of the slip velocity on boundary $\Sigma$ (the inner streaming velocity distribution on $\Sigma$), and the x component ($u_{outer}$) and z component ($v_{outer}$) of the outer streaming velocity in $\Omega_o$. The results of the convergence functions for these physics are plotted in Fig. S3 as a function of inner streaming domain thickness (h). The values of the convergence functions for these physics exhibit a similar tendency to decrease to the minimum at $2.5\delta_v \le h \le 4\delta_v$ and they start to increase again. The convergence functions variation around this range where the optimal h value locates is zoomed in and plotted in Fig. S3(b). As shown in this figure, for the inner acoustic streaming in domain $\Omega_i$, the horizontal component $u_2$ has a minimum convergence function value of 0.05602 at h=$3.2\delta_v$ and the vertical component $v_2$ has a minimum convergence function value of 0.15873 at h=$3.4\delta_v$. Exploring
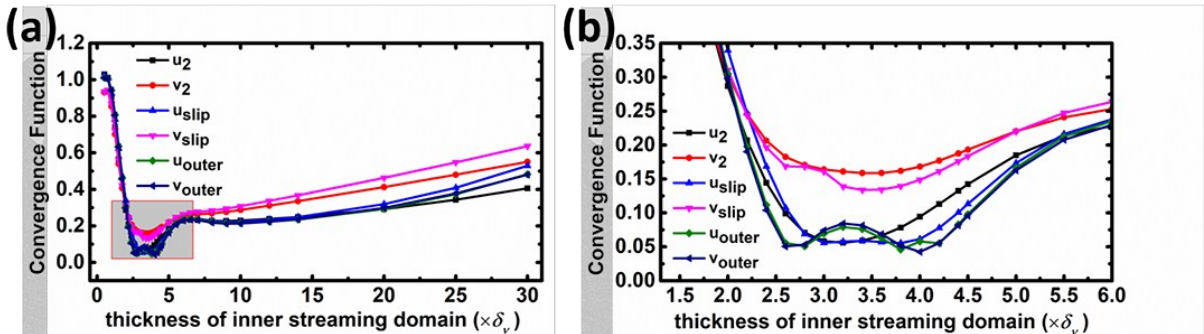


**Fig. S3** The change of the convergence function of inner streaming velocity components ($u_2$ and $v_2$ in $\Omega_i$), slip velocity components ($u_{slip}$ and $v_{slip}$ on $\Sigma$) and the outer streaming velocity components ($u_{outer}$ and $v_{outer}$ in $\Omega_o$) with respect to h, the thickness of the inner streaming domain. The horizontal coordinate is the times of the h to the $\delta_v$ (0.147 $\mu m$ in this study). The convergence of the x component of outer streaming ($u_{outer}$) and the z component of the outer streaming ($v_{outer}$) in the outer streaming domain ($\Omega_o$) reach their minimums of 0.04594 and 0.04256 when h=$3.8\delta_v$ and h=$4\delta_v$, respectively. This result indicates that setting h=$4\delta_v$ in the slip velocity

the slip velocity, the convergence function of the horizontal component $u_{slip}$ reaches a minimum of 0.05547 at h=3.8$\delta_v$ and the vertical component $v_{slip}$ reaches to the minimum of 0.13386 at h=3.4$\delta_v$. According to this data, we discover that the slip velocity method yields a better approximation for the horizontal velocity component in $\Omega_i$ than the vertical velocity component. The boundary condition on $\Sigma$ might not totally match the real situation. Since the horizontal streaming velocity dominates in the inner streaming domain, the approximation of the vertical component is not as good as the horizontal one, although it does not much affect the outer streaming calculation. Analyzing the outer streaming velocity components, a goal of this study, the minimum convergence function value of $u_{outer}$ appears at h=3.8$\delta_v$ as 0.04594, and the minimum convergence function value of $v_{outer}$ appears at h=4$\delta_v$ as 0.04256. Thus, setting h to ~4$\delta_v$ in the slip velocity method yields the best approximation to traditional research. As shown in Fig. S2(d), the amplitude of the mass source term and the curl of the force source term also vanish close to zero at ~4$\delta_v$. If the inner streaming domain is thinner than ~4$\delta_v$, the effective mass source and force source terms cannot be taken into simulation completely. If the inner streaming domain gets thicker than ~4$\delta_v$, the horizontal component of the slip velocity will greatly decrease from its maximum, and the vertical component of the slip velocity will increase. This will make the amplitude of the outer streaming smaller than the solution of the traditional solution. Here, as we set the thickness of the inner streaming domain to h=4$\delta_v$, the convergence function values of $u_{outer}$ and $v_{outer}$ are in the $10^{-2}$ order, which indicates an approximation close to the reference solution.[1] Thus, we determine the optimal thickness of the inner streaming domain ($\Omega_i$) as 4$\delta_v$ and use this setting in the 3D simulation of the IDT-induced acoustic streaming. Based on this setting, the "slip velocity method" takes 1227 s to solve the 2D acoustic streaming shown in Fig. S1, while the traditional approach takes 2620 s to solve the same case. According to this, we estimate that the "slip velocity method" could save the computation time by 53% compared to the traditional approach.

**Part 2. Additional Figures and Movies for the Main Text**
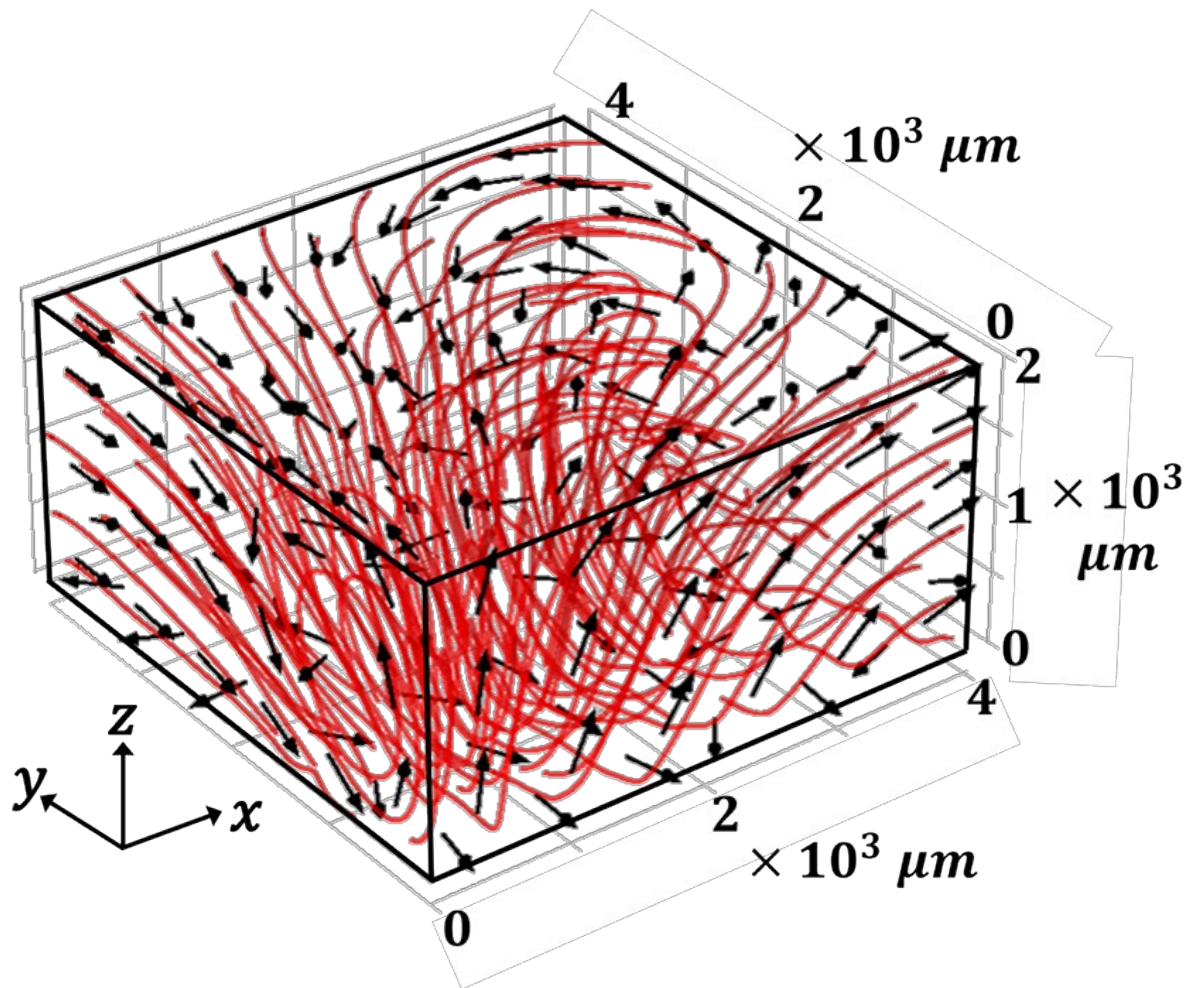


**Fig. S4** Simulated 3D acoustic streaming pattern activated by a quarter of the IDT in the domain shown in Fig. 2(a). The red lines and black arrows show the streamlines and acoustic streaming directions. This is an enlargement of Fig. 4(a).
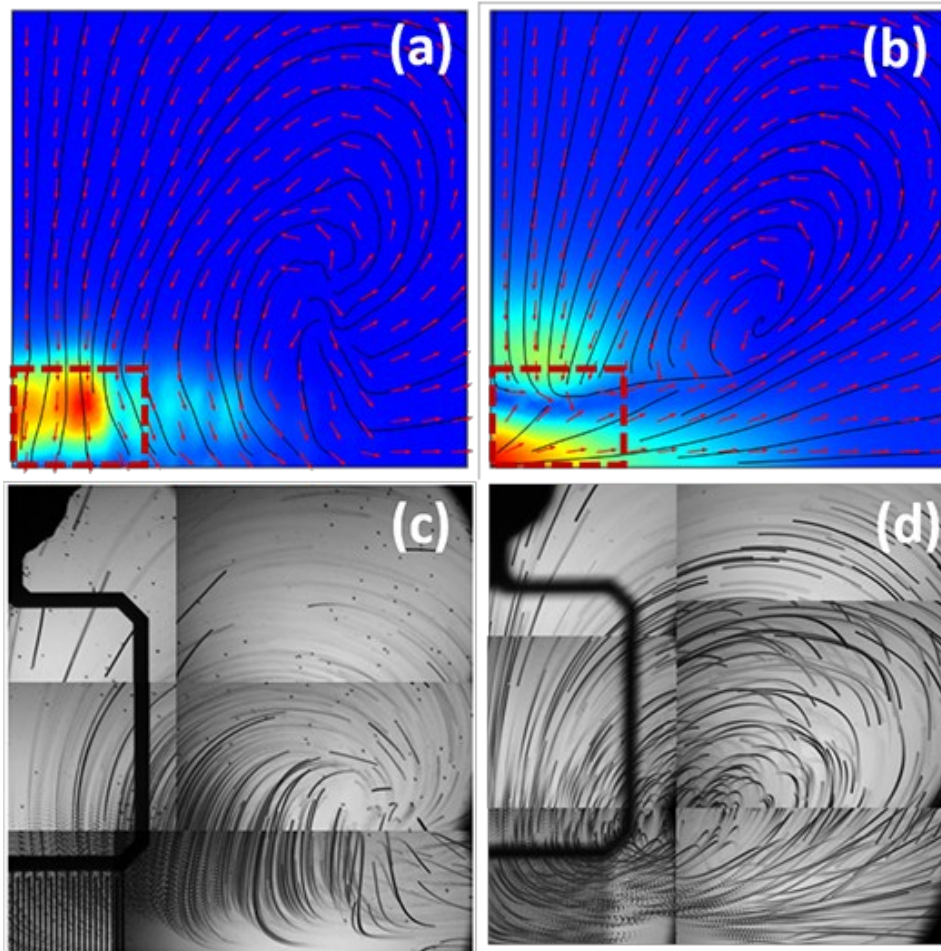
**Fig. S5** Simulation and experimental results which show the acoustic streaming patterns in the x-y planes at different depths, as induced by a quarter of an IDT. (a) and (b) Simulated acoustic streaming patterns at z=100 µm and z=1000 µm planes. The red frames represent the IDT area. The red color and blue color in the background indicate the high and low magnitudes of the streaming velocities, respectively. The black lines and red arrows show, respectively, the streamline and streaming direction of the acoustic streaming patterns. (c) and (d) Experimentally measured acoustic streaming patterns at z=100 µm and z=1000 µm planes.

**Movie S1** Simulation result of droplet trajectories in the x-y-2000 µm plane driven by the 2D streaming pattern in Fig. 4(b). This movie corresponds to Fig. 5(a).

**Movie S2** Experimentally observed droplet trajectory when the droplet was released from the initial position in Fig. 5(b). The movie was recorded with a high-speed camera at a frame rate of 250 fps.

**Movie S3** Experimentally observed droplet trajectory when the droplet was released from the initial position in Fig. 5(c). The movie was recorded by a high-speed camera at a frame rate of 250 fps.

**Movie S4** Multi-step droplet manipulation achieved by a device with a 1×10 IDT array. This movie corresponds to Fig. 6. The movie is in real time.

# References

1    N. Nama, R. Barnkob, Z. Mao, C. J. Kähler, F. Costanzo and T. J. Huang, *Lab Chip*, 2015, **15**, 2700–2709.

2    F. Guo, Z. Mao, Y. Chen, Z. Xie, J. P. Lata, P. Li, L. Ren, J. Liu, J. Yang, M. Dao, S. Suresh and T. J. Huang, *Proc. Natl. Acad. Sci.*, 2016, **113**, 1522–1527.

3    S. S. Sadhal, *Lab Chip*, 2012, **12**, 2292–2300.

4    M. Wiklund, R. Green and M. Ohlin, *Lab Chip*, 2012, **12**, 2438–2451.